1

Synchrotron Light Sources

Zhentang Zhao

Shanghai Synchrotron Radiation Facility, Shanghai Institute of Applied Physics, Chinese Academy of Sciences, 239 Zhangheng Road, Pudong New District, Shanghai, 201204, China

1.1 Introduction

Synchrotron light sources or storage ring light sources are indispensable large-scale scientific tools for basic and applied frontier research in various fields, ranging from materials science, energy science, life science, environmental science, to archaeological applications. Their development has evolved from the first generation to the third generation in the past five decades, and has now entered into the fourth generation phase with even higher brightness and coherence radiation based on the diffraction limited storage ring concept. Currently, there are over 50 synchrotron light sources in operation in more than 20 countries, and over 15 new synchrotron radiation facilities have been set up worldwide in various stages of commissioning, construction, design, or planning. In this chapter, we will introduce the basics of synchrotron radiation generation, storage ring physics, and radiation characteristics, which are of interest to synchrotron radiation users. We will also present the current status of the storage ring light source development across the world. This chapter is intended to cover only the basic concepts of synchrotron light source and review the current status on its development. For readers who are interested in the detailed physics and related technologies, we recommend the books or monographs in Refs [1–15].

1.2 Synchrotron Radiation Generation

When a relativistic electron moves on a curved path at nearly the speed of light, it emits electromagnetic radiation. This radiation was theoretically predicated and studied by Lienard, Wiechert, and Schott in around 1900, and its visible part was first observed at the 70 MeV GE electron synchrotron in 1947. Since then, this electromagnetic radiation has been called synchrotron radiation.

Synchrotron, a kind of circular particle accelerator, can accelerate charged particles from low energy to high energy or keep the particles circulating on the

Synchrotron Radiation in Materials Science: Light Sources, Techniques, and Applications, First Edition.
Edited by Chunhai Fan and Zhentang Zhao.

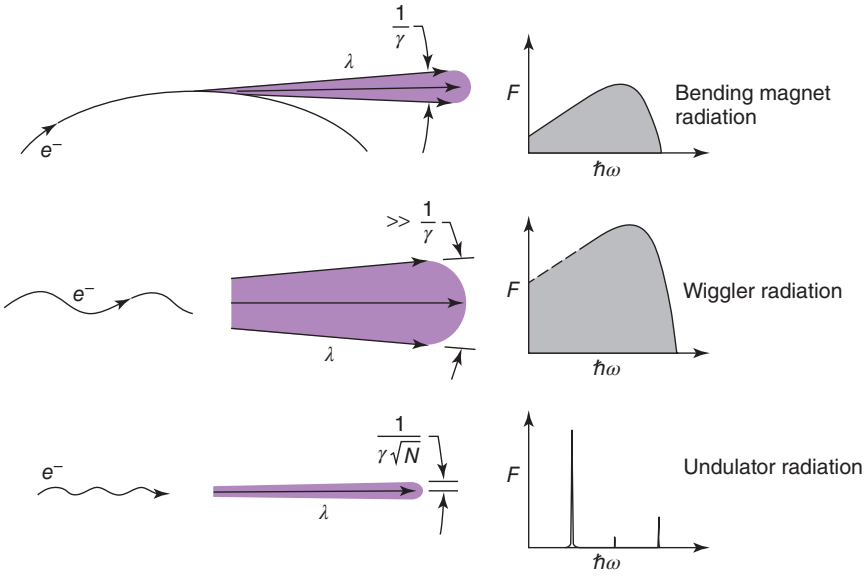

Figure 1.1 Synchrotron radiation from bending magnets, wigglers, and undulators [3]. (Cambridge University Press.)

circular orbit at a constant energy for hours and days, which is referred to as storage ring. The electron storage ring is the core part of synchrotron light source. Relativistic electrons, circulating in the storage ring, generate synchrotron radiation when passing through three on-path major source components: the bending magnet, wiggler, and undulator magnets, as shown in Figure 1.1.

This synchrotron radiation is extremely intense over a broad range of wavelengths from infrared through the visible and ultraviolet range, to the soft and hard X-ray part of the electromagnetic spectrum. Bending magnet radiation has broad spectrum and good photon flux; wiggler radiation provides higher photon energies and more photon flux; and undulator provides brighter radiation with smaller spot size and partial coherence.

1.2.1 Radiation from Bending Magnet

A bending magnet, also called a dipole magnet, consists of opposite poles, namely the north and south poles, which are on opposite sides of the magnet providing a homogeneous magnetic field.

As shown in Figure 1.2, when a relativistic electron of energy E travels on a circular trajectory in a dipole magnet of main field $B_y = B$ and bending radius ρ, where $G = B\rho = p/e$, the ratio of momentum to charge, is often called the magnetic rigidity, it radiates electromagnetic power confined in a cone with $\pm 1/\gamma$ opening toward its moving direction. Its radiation power can be expressed as,

$$P_s = \frac{2}{3} r_0 m_0 c^2 \frac{c\beta^4\gamma^4}{\rho^2},$$

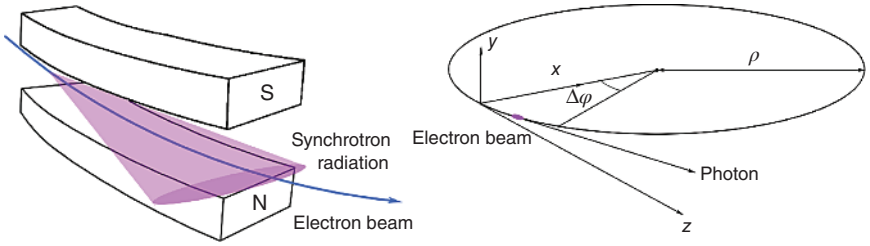

Figure 1.2 Synchrotron radiation from bending magnet.

where e is the electron charge, m_0 is the electron rest mass, βc is the electron moving speed, $\gamma = E/(m_0c^2)$ is the Lorentz factor, and $r_0 = e^2/(4\pi\epsilon_0 m_0 c^2)$ is the electron classical radius. Integrating the radiated power over an isomagnetic storage ring with constant ρ gives an electron energy loss in one turn due to the synchrotron radiation as follows,

$$U_0 = \frac{4\pi}{3} r_0 m_0 c^2 \beta^3 \frac{\gamma^4}{\rho}.$$

In engineering units,

$$U_0[\text{keV}] = 88.5 \frac{E^4[\text{GeV}]}{\rho[\text{m}]}.$$

For an electron beam traveling through a dipole magnet of bending angle $\Delta\varphi$ with average current of I_b, the radiated power is,

$$P_d = \frac{2}{3} r_0 m_0 c^2 \frac{c\beta^4\gamma^4}{e\rho} \Delta\varphi I_\text{b}.$$

For an electron beam circulating in storage ring (with average current of I_b and revolution time of T_0), the total radiated power per turn is,

$$P_0 = \frac{I_\text{b} U_0}{e} = \frac{4\pi}{3} r_0 m_0 c^2 \beta^3 \frac{\gamma^4}{e\rho} I_\text{b}.$$

When an electron travels on the circular path in a dipole magnet, its emitting radiation on a fixed target outside the orbit circle comes only from a short arc of electron trajectory, this short synchrotron radiation pulse covers a wide continuous spectrum of photon energies from infrared to X-rays depending on the electron energy and the bending magnetic field. A so-called critical photon energy ε_c (or critical frequency ω_c) is defined as the photon energy which divides the synchrotron radiation into two spectral regions with equal radiated power,

$$\omega_\text{c} = \frac{3}{2} c \frac{\gamma^3}{\rho},$$

$$\varepsilon_\text{c} = \frac{h}{2\pi}\omega_\text{c} = \frac{3hc}{4\pi}\frac{\gamma^3}{\rho}.$$

In engineering units,

$$\varepsilon_\text{c}[\text{keV}] = 0.665 E^2[\text{GeV}] B[\text{T}].$$

The significance of the critical photon energy is that it sets up the upper bund for the synchrotron radiation spectrum, and the spectral power falls rapidly for

photon energies above this critical value. The complete spectral distribution of synchrotron radiation can be calculated using the Fourier transform of the radiation electric field,

$$\frac{dP_s}{d\omega} = \frac{P_s}{\omega_c} S\left(\frac{\omega}{\omega_c}\right),$$
$$S\left(\frac{\omega}{\omega_c}\right) = \frac{9\sqrt{3}}{8\pi}\frac{\omega}{\omega_c}\int_{\omega/\omega_c}^{\infty} K_{5/3}(x)dx.$$

The $K_{5/3}(x)$ above and $K_{2/3}(x)$ below are the modified Bessel functions. The on-axis spectral photon flux $\dot{N}_{\mathrm{ph}}$ (defined as the number of photons per unit time) per unit solid angle in a bandwidth $\Delta\omega/\omega$ and for a circulating beam current I_b is a more useful parameter. It can be written as,

$$\frac{d\dot{N}_{\mathrm{ph}}}{d\Omega} = \frac{d^2\dot{N}_{\mathrm{ph}}}{d\theta d\psi} = \frac{3\alpha E^2 I_b}{4\pi^2 e(mc^2)^2}\frac{\Delta\omega}{\omega}\left(\frac{\omega}{\omega_c}\right)^2 K_{2/3}^2\left(\frac{\omega}{2\omega_c}\right),$$

where $\alpha = e^2/(2ch\varepsilon_0)$ is the fine structure constant. In engineering units, and with 0.1% bandwidth,

$$\frac{d\dot{N}_{\mathrm{ph}}}{d\Omega}[\mathrm{photons/sec/mrad^2}] = 1.33\times 10^{13} E^2\,[\mathrm{GeV}] I_b\,[\mathrm{A}]\left(\frac{\omega}{\omega_c}\right)^2 K_{2/3}^2\left(\frac{\omega}{2\omega_c}\right).$$

The on-axis photon flux per unit deflection angle is,

$$\frac{d\dot{N}_{\mathrm{ph}}}{d\psi} = \frac{P_s}{\omega_c h}\frac{\Delta\omega}{\omega} S\left(\frac{\omega}{\omega_c}\right).$$

The photon flux at energy ε is given by,

$$\dot{N}_{\mathrm{ph},\varepsilon} = \frac{P_s}{\varepsilon_c \varepsilon} S\left(\frac{\omega}{\omega_c}\right) = \frac{9\sqrt{3}\pi}{2}\frac{P_s}{h^2\omega_c^2}\int_{\omega/\omega_c}^{\infty} K_{5/3}(\bar{x})d\bar{x}$$

and by integrating the photon flux for ε from zero to infinity, the total number of radiating photons per unit time is,

$$\dot{N}_{\mathrm{ph}} = \int_0^{+\infty} \dot{N}_{\mathrm{ph},\varepsilon} d\varepsilon = \frac{15\sqrt{3}}{8}\frac{P_s}{\varepsilon_c}.$$

The total photon flux at energy ε for the storage ring with average beam current I_b is,

$$\dot{N}_{\mathrm{ph},\varepsilon} = \frac{3\sqrt{3}}{2}\frac{r_0 m_0 c^2 \beta^3 \gamma^4}{e\rho\varepsilon_c^2} I_b \int_{\omega/\omega_c}^{\infty} K_{5/3}(\bar{x})d\bar{x}.$$

The total photon flux

$$\dot{N}_{\mathrm{ph}} = \frac{5\pi\sqrt{3}}{2e\varepsilon_c} r_0 m_0 c^2 \beta^3 \frac{\gamma^4}{\rho} I_b.$$

1.2.2 Radiation from Undulator

Undulator and wiggler, or so-called insertion devices, consisting of a series of alternating magnet poles, deflect the electron periodically in opposite directions. They are installed in the storage ring straight sections and optimized for generating specific synchrotron radiation characteristics.

1.2.2.1 Planar Undulator Radiation

The radiation from planar undulator with N_u period has the same physical process as a short bending magnet, but the N_u times of oscillations that an electron performs in an undulator transform the radiation into quasi-monochramatic with finite line width and within a cone of $1/(\gamma N_u^{1/2})$. This makes the planar undulator radiation intensity effectively enhanced with reasonable radiation power (Figure 1.3).

In a planar undulator with period length λ_u and peak field B_0, the main magnetic field is $B_y = B_0 \sin(2\pi s/\lambda_u)$, and the average instantaneous radiation power of an electron traveling in planar undulator is,

$$P_u = \frac{r_0 c m_0 c^2 \gamma^2 K^2}{3}\left(\frac{2\pi}{\lambda_u}\right)^2,$$

where K is the so-called deflection parameter and is defined as,

$$K = \frac{ecB_0\lambda_u}{2\pi m_0 c^2}.$$

The total energy emitted by an electron from the undulator with a length of $L_u = N_u\lambda_u$ is,

$$U_u = \frac{r_0 m_0 c^2 \gamma^2 K^2 L_u}{3}\left(\frac{2\pi}{\lambda_u}\right)^2.$$

The total average radiated power of an electron beam with current of I_b passing through the undulator is,

$$P_{u,I} = \frac{r_0 m_0 c^2 \gamma^2 K^2 L_u I_b}{3e}\left(\frac{2\pi}{\lambda_u}\right)^2.$$

In engineering units,

$$P_{u,I}\,[\mathrm{kW}] = 0.633 E^2\,[\mathrm{GeV}] B_0^2\,[\mathrm{T}] L_u[\mathrm{m}] I_b\,[\mathrm{A}].$$

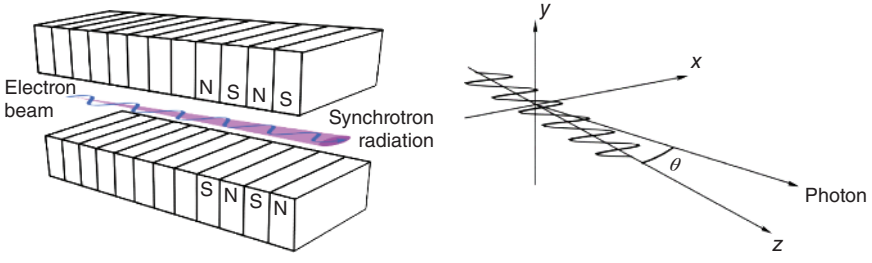

Figure 1.3 Synchrotron radiation from undulator.

Owing to the cooperative effect of radiation from different periods, the undulator radiation has line spectral characteristics. Its radiation wavelength, or photon energy at the nth harmonic, can be expressed as,

$$\lambda_n = \frac{\lambda_u}{2n\gamma^2}\left(1 + \frac{1}{2}K^2 + \gamma^2\theta^2\right)$$

with the line width,

$$\frac{\Delta\omega_n}{\omega_n} = \frac{1}{nN_u},$$

where $n = 1, 3, 5, \ldots$ is the harmonic number of radiation line, $\omega_n = 2\pi c/\lambda_n$, $\Delta\omega_n = \omega - n\omega_1$.

In the storage ring with circulating current I_b, the total on-axis undulator photon flux per unit solid angle is,

$$\frac{d\dot{N}_{ph}}{d\Omega} = \sum_{n=1}^{\infty}\frac{d\dot{N}_{ph,n}}{d\Omega} = \alpha\gamma^2 N_u^2\frac{I_b}{e}\sum_{n=1}^{\infty}\frac{\Delta\omega}{\omega}\left(\frac{\sin\left(\frac{\pi N_u\Delta\omega_n}{\omega_1}\right)}{\frac{\pi N_u\Delta\omega_n}{\omega_1}}\right)^2 A_n(K)$$

$$A_n(K) = \frac{n^2K^2}{(1+K^2/2)^2}\left[J_{(n+1)/2}\left(\frac{nK^2}{4+2K^2}\right) - J_{(n-1)/2}\left(\frac{nK^2}{4+2K^2}\right)\right]^2,$$

where $\alpha = e^2/(2\varepsilon_0 hc)$ is called the fine structure constant and $J_m(k)$ is the Bessel function. In one measurement of a typical experiment, only one harmonic radiation is directed to the sample, and therefore, the radiation characteristics at specific wavelength and its tuning range is of great significance. As a more important parameter, the on-axis photon flux per unit solid angle at the nth harmonic is,

$$\frac{d\dot{N}_{ph,n}}{d\Omega} = \alpha\gamma^2 N_u^2\frac{I_b}{e}\frac{\Delta\omega}{\omega}\left(\frac{\sin\left(\pi N_u\Delta\omega_n/\omega_1\right)}{\pi N_u\Delta\omega_n/\omega_1}\right)^2 A_n(K).$$

The on-axis photon flux at the nth harmonic is,

$$\dot{N}_{ph,n} = \pi\alpha N_u\frac{I_b}{e}\frac{\Delta\omega}{\omega_n}\frac{1+K^2/2}{n}A_n(K).$$

In engineering units of per 0.1% bandwidth,

$$\dot{N}_{ph,n}[\text{photons/sec}] = 1.43\times10^{14}N_u I_b[\text{A}]\frac{1+K^2/2}{n}A_n(K).$$

1.2.2.2 Helical Undulator Radiation

The helical undulator has both horizontal and vertical field components, $B_x = B_{x0}\sin(2\pi s/\lambda_u - \phi)$ *and* $B_y = B_{y0}\sin(2\pi s/\lambda_u)$, which periodically vary in a sine wave with a period of λ_u along its longitudinal direction. It is widely used for generating circularly or elliptically polarized radiation. Its horizontal and vertical deflection parameters are defined as,

$$K_x = \frac{ecB_{x0}\lambda_u}{2\pi m_0c^2}, \quad K_y = \frac{ecB_{y0}\lambda_u}{2\pi m_0c^2}.$$

The radiation wavelength of nth harmonics is,

$$\lambda_n = \frac{\lambda_\mathrm{u}}{2n\gamma^2}\left(1 + \frac{1}{2}K_x^2 + \frac{1}{2}K_y^2 + \gamma^2\theta^2\right).$$

Its average instantaneous radiation power is,

$$P_\mathrm{hu} = \frac{r_0 c m_0 c^2 \gamma^2 \left(K_x^2 + K_y^2\right)}{3}\left(\frac{2\pi}{\lambda_\mathrm{u}}\right)^2.$$

The total radiated energy of an electron passing through a helical undulator is,

$$U_\mathrm{hu} = \frac{r_0 m_0 c^2 \gamma^2 \left(K_x^2 + K_y^2\right) L_\mathrm{u}}{3}\left(\frac{2\pi}{\lambda_u}\right)^2$$

and the total average radiated power of an electron beam I_b passing through the helical undulator is,

$$P_{\mathrm{hu},I} = \frac{r_0 m_0 c^2 \gamma^2 \left(K_x^2 + K_y^2\right) L_\mathrm{u} I_\mathrm{b}}{3e}\left(\frac{2\pi}{\lambda_\mathrm{u}}\right)^2.$$

In engineering units,

$$P_{\mathrm{hu},I}\,[\mathrm{kW}] = 0.633E^2\,[\mathrm{GeV}]\left(B_{x0}^2 + B_{y0}^2\right)[\mathrm{T}]L_\mathrm{u}\,[\mathrm{m}]\,I_\mathrm{b}\,[\mathrm{A}].$$

The total on-axis photon flux per unit solid angle is,

$$\frac{d\dot{N}_\mathrm{ph}}{d\Omega} = \alpha\gamma^2\left(K_x^2 + K_y^2\right)N_\mathrm{u}^2\frac{I_\mathrm{b}}{e}\frac{\Delta\omega}{\omega}.$$

The on-axis photon flux at nth harmonic per unit solid angle is,

$$\frac{d\dot{N}_{\mathrm{ph},n}}{d\Omega} = \alpha\gamma^2 N_\mathrm{u}^2\frac{I_\mathrm{b}}{e}\frac{\Delta\omega}{\omega}\left(\frac{\sin\left(\pi N_\mathrm{u}\Delta\omega_n/\omega_1\right)}{\pi N_\mathrm{u}\Delta\omega_n/\omega_1}\right)^2 A_n(K_x, K_y)$$

$$A_n(K_x, K_y) = \frac{n^2}{(1 + K_x^2/2 + K_y^2/2)^2}\left\{K_x^2[J_{(n+1)/2}(Z) + J_{(n-1)/2}(Z)]^2 + K_y^2[J_{(n+1)/2}(Z) - J_{(n-1)/2}(Z)]^2\right\}$$

$$Z = \frac{n(K_y^2 - K_x^2)}{4 + 2(K_x^2 + K_y^2)}.$$

The on-axis photon flux at nth harmonic is,

$$\dot{N}_{\mathrm{ph},n} = \pi\alpha N_\mathrm{u}\frac{I_\mathrm{b}}{e}\frac{\Delta\omega}{\omega_n}\frac{1 + K_x^2/2 + K_y^2/2}{n}A_n(K_x, K_y).$$

In engineering units,

$$\dot{N}_{\mathrm{ph},n}[\mathrm{photons/sec}] = 1.43 \times 10^{14} N_\mathrm{u} I_\mathrm{b}[\mathrm{A}]\frac{1 + K_x^2/2 + K_y^2/2}{n}A_n(K_x, K_y).$$

When $K_{\mathrm{hu}} = K_x = K_y$, $\phi = \pi/2$, the helical undulator radiation is purely circularly polarized, the radiation at fundamental wavelength is,

$$\lambda_1 = \frac{\lambda_{\mathrm{u}}}{2\gamma^2}(1 + K_{\mathrm{hu}}^2 + \gamma^2\theta^2).$$

The total average radiated power from the helical undulator is,

$$P_{\mathrm{hu},I} = \frac{2r_0 m_0 c^2 \gamma^2 K_{\mathrm{hu}}^2 L_{\mathrm{u}} I_{\mathrm{b}}}{3e}\left(\frac{2\pi}{\lambda_{\mathrm{u}}}\right)^2.$$

In engineering units,

$$P_{\mathrm{hu},I}\,[\mathrm{kW}] = 1.266E^2\,[\mathrm{GeV}]B_0^2\,[\mathrm{T}]L_{\mathrm{u}}\,[\mathrm{m}]I_{\mathrm{b}}\,[\mathrm{A}].$$

The on-axis photon flux (containing only fundamental wavelength) is,

$$\dot{N}_{\mathrm{ph},1}[\mathrm{photons/sec}] = 2.86 \times 10^{14} N_{\mathrm{u}} I_{\mathrm{b}}[\mathrm{A}]\frac{K_{\mathrm{hu}}^2}{1 + K_{\mathrm{hu}}^2}.$$

1.2.3 Radiation from Wiggler

A wiggler is a set of strong dipole magnets with alternating polarity, located in a straight section with no deflection and displacement to the beam passing through from the entrance to exit. Wigglers are classified into two types, wavelength shifter and multipole wiggler. The wavelength shifter, with a short and strong bending magnet in the center and weak magnets at the ends, has the same radiation properties as that from the bending magnets of the storage ring, but it can push up the critical photon energy with its high field. The multipole wiggler is a special kind of undulator with N_{w} longer period of λ_{w} and large $K_{\mathrm{w}}(K_{\mathrm{w}} \gg 1)$, and its radiation is confined in a cone of K_{w}/γ. The large value of K_{w} (strong field) makes the multipole wigglers exhibit a significant difference in radiation spectrum property compared with undulators, it has strong interference effects in the fundamental and first few harmonics, but appears as a smooth spectrum that is similar to that of a bending magnet at high frequency. Therefore, a wiggler is often used to provide an enhanced performance from a super bending magnet; its multipoles and higher magnetic field result in much higher radiation intensity and higher critical photon energy. Furthermore, the multipole wiggler is not only used for delivering high flux but also for providing polarized radiation. The instantaneous radiation power of an electron passing through the multipole wiggler can be written as,

$$P_{\mathrm{w}} = \frac{r_0 c m_0 c^2 \gamma^2 K_{\mathrm{w}}^2}{3}\left(\frac{2\pi}{\lambda_{\mathrm{w}}}\right)^2$$

with

$$K_{\mathrm{w}} = \frac{ecB_0\lambda_{\mathrm{w}}}{2\pi m_0 c^2}.$$

The total energy emitted from an electron from the wiggler with a length of $L_{\mathrm{w}} = N_{\mathrm{w}}\lambda_{\mathrm{w}}$ is,

$$U_{\mathrm{w}} = \frac{r_0 e^2 \gamma^2 B_0^2 L_{\mathrm{w}}}{3m_0}.$$

The total average radiated power of an electron beam I_b passing through the wiggler is,

$$P_{w,I} = \frac{r_0 e\gamma^2 B_0^2 L_w I_b}{3m_0}.$$

In engineering units,

$$P_{w,I}\,[\mathrm{kW}] = 0.633E^2\,[\mathrm{GeV}]B_0^2\,[\mathrm{T}]L_w\,[\mathrm{m}]I_b\,[\mathrm{A}].$$

The on-axis radiated power per solid angle,

$$\frac{dP}{d\Omega} = \frac{21\gamma^2}{16\pi K_w} P_{w,I} G(K_w)$$

$$G(K_w) = \frac{K_w(K_w^6 + 24K_w^4/7 + 4K_w^2 + 16/7)}{(1+K_w^2)^{7/2}}.$$

Wigglers have the similar radiation spectral characteristics, which can be calculated using the formulae derived for bending magnet radiation. At the same magnetic field, the wiggler radiation power is $2N_w$ times of that from the bending magnet. With higher magnetic field, wigglers can push up the critical photon energy and produce higher radiation power.

1.3 Light Source Storage Ring and Its Beam Dynamics

A typical storage ring light source complex consists of an injector, a storage ring, and dozens of beamlines and experimental stations. The injector usually comprises either a 50–300 MeV electron linac followed by a booster synchrotron accelerating electrons to the storage ring energy or a full energy electron linac. Most storage rings are operated at fixed energy, although there are a few of them that need to ramp their injecting energy from low to the working one for employing a low-cost injector in storage ring light sources. Figure 1.4 shows the layout of the Shanghai Synchrotron Radiation Facility (SSRF) complex, which consists of a 150 MeV linac, a full energy booster, and a 3.5 GeV storage ring, and currently 31 beamlines and 45 experimental stations are under operation and construction.

The storage ring is the core part of the light source. It defines various radiation source properties, such as spectral range, flux, brightness, time structure, and coherence. By using the typical parameters of the SSRF, Figure 1.5 shows the calculation results of the flux and brightness for various types of radiation sources, including bending magnet, wigglers, and undulators.

Normally, light source storage rings contain five major technical systems that affect its beam properties, (i) a magnet system, including dipoles, quadrupoles, and sextupoles, to constitute the ring magnetic lattice for controlling the electron orbit and beam properties, (ii) an RF system to compensate the energy loss of the circulating beam due to synchrotron radiation, (iii) a vacuum system to keep the electrons moving in an environment with air pressure of $\sim 10^{-8}$ Pa for reducing the collision of circulating electrons with the residual molecules, (iv) an injection system to fill the storage ring with new electrons, and (v) insertion devices, such

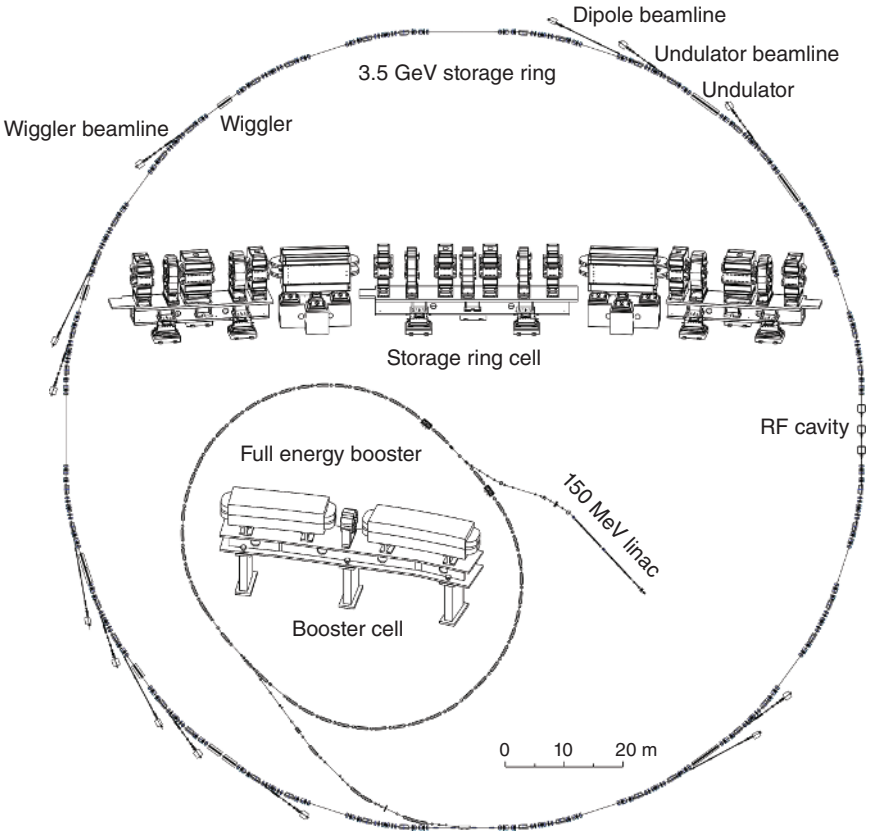

Figure 1.4 The SSRF accelerator complex (150 MeV Linac, full energy booster, and 3.5 GeV storage ring).

as undulators and wigglers, to generate high brightness, high flux, or high photon energy synchrotron radiation that is required for various synchrotron radiation experiments.

1.3.1 Transverse Dynamics

There exists a closed sequence of dipole and quadruple magnets connected by field-free straight sections along the complete storage ring, which determines a stable transverse motion of the electrons that repeat their revolutions around a reference orbit, the so-called closed orbit. This closed magnet sequence, called the magnet lattice, is a periodic magnetic structure layout, composed of dozens of basic units called cells, which can be typed as the double-bend achromat (DBA), the triple-bend achromat (TBA), the quadrupole-bend achromat (QBA) or the multi-bend achromat (MBA). In a storage ring, the dipole magnets make the relativistic electron follow a circular path during the travel of their uniform fields that are perpendicular to the velocity of electrons; quadrupole magnets, with

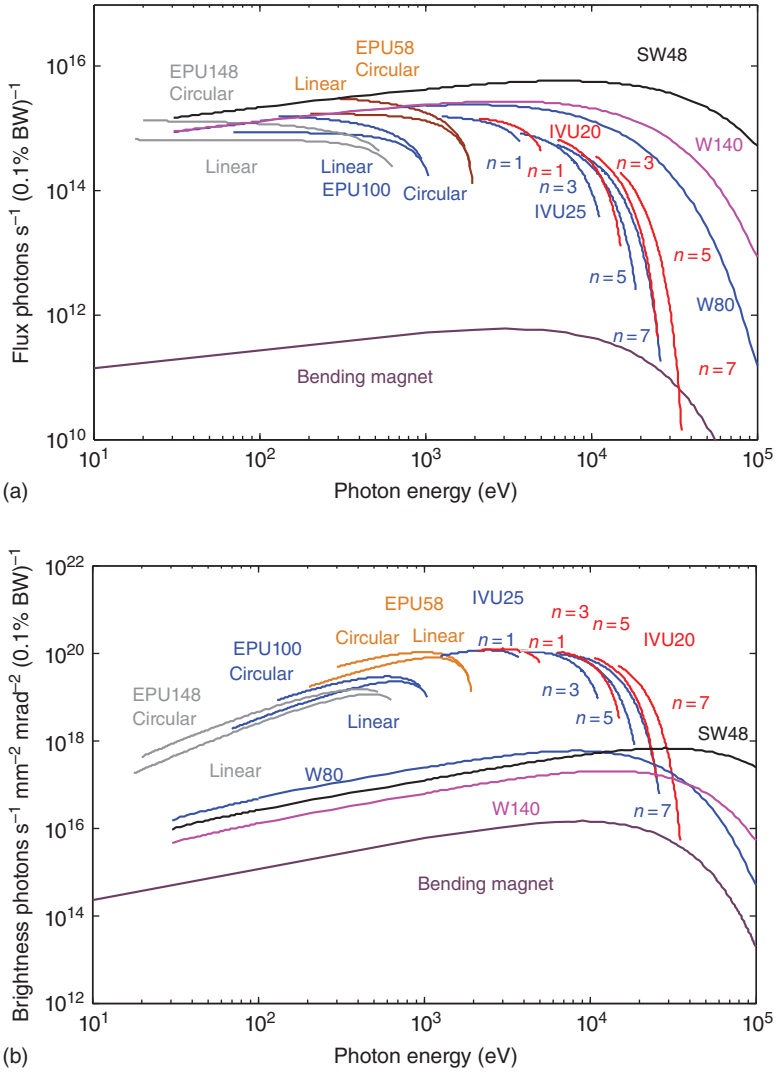

Figure 1.5 The output radiation flux (a) and brightness (b) of the SSRF storage ring (at the electron energy of 3.5 GeV and beam current of 300 mA).

their magnetic field components, are a linear function of the beam displacement from the magnet axis, focus, or defocus electrons to keep them stably moving in a confined transverse region along the ring.

For a storage ring of given energy E, the on-energy electrons will move on a so-called synchronous orbit. The energy of these synchronous electrons has the following relation with the storage ring bending magnet field,

$$E = \frac{ec}{\beta} B\rho.$$

where B is the bending field and ρ is the radius of the electron path curve in the bending field. In engineering units, for β is close to 1,

$$E\,[\mathrm{GeV}] = 0.3B\,[\mathrm{T}]\rho\,[\mathrm{m}].$$

The on-energy electron makes a transverse motion on the synchronous orbit. Its betatron oscillation, transverse displacements from the closed orbit, in horizontal plane x and vertical plane y can be expressed as,

$$\begin{aligned}
x_\beta(\mathrm{s}) &= \sqrt{\varepsilon_x \beta_x(s)}\cos[\phi_x(s) + \phi_{0x}] \\
x'_\beta(\mathrm{s}) &= \sqrt{\frac{\varepsilon_x}{\beta_x(s)}}\left(\frac{\beta'_x(s)}{2}\cos[\phi_x(s) + \phi_{0x}] - \sin[\phi_x(s) + \phi_{0x}]\right) \\
y_\beta(\mathrm{s}) &= \sqrt{\varepsilon_y \beta_y(s)}\cos[\phi_y(s) + \phi_{0y}] \\
y'_\beta(\mathrm{s}) &= \sqrt{\frac{\varepsilon_y}{\beta_y(s)}}\left(\frac{\beta'_y(s)}{2}\cos[\phi_y(s) + \phi_{0y}] - \sin[\phi_y(s) + \phi_{0y}]\right) \\
\phi_{x,y} &= \int_0^s \frac{ds}{\beta_{x,y}(s)} \\
\nu_{x,y} &= \frac{1}{2\pi}\int_0^C \frac{ds}{\beta_{x,y}(s)},
\end{aligned}$$

where ε_x and ε_y are the electron emittances in x (horizontal) and y (vertical) directions, $\beta_x(s)$ and $\beta_y(s)$ are the beta functions, $\phi_{0x,0y}$ are the initial phases of the beam motion respectively, and C is the circumference of the storage ring.

Emittance is a phase space expression of electron distribution. In transverse planes, it represents the phase space area of the beam size multiplied by the magnitude of divergence. Emittance remains unchanged as electrons circulate in the storage ring if no acceleration, horizontal–vertical coupling change, or beam instabilities occur. Beta functions represent the amplitudes of electron oscillation in horizontal and vertical planes at the position s. They appear in periodic variations along s under the periodic magnetic lattice condition. Their relations are,

$$\varepsilon_{x0} = \gamma_x(s)x^2 + 2\alpha_x(s)xx' + \beta_x(s)x'^2,$$

where

$$\begin{aligned}
\alpha_x(s) &= -\frac{\beta'_x(s)}{2} \\
\gamma_x(s) &= \frac{1 + \alpha_x^2(s)}{\beta_x(s)}.
\end{aligned}$$

For the off-energy electrons, they will move on a nonsynchronous orbit that is characterized by two important physical quantities, dispersion η and chromaticity ξ. The dispersion function describes the closed orbit of the off-energy electrons in the ring, which usually exists only in the horizontal plane due to no bending field in the vertical direction, and it is defined as,

$$x_\varepsilon = \eta(s)\frac{\Delta E}{E}.$$

In such condition, the electron motion in the horizontal plane can be decomposed into two parts as in the following,

$$x(s) = x_\epsilon + x_\beta = \eta(s)\frac{\Delta E}{E} + \sqrt{\epsilon_x \beta_x(s)}\cos[\phi_x(s) + \phi_{0x}].$$

The quadrupole magnets exert focusing force on the electrons, which is inversely proportional to the electron energy; this so-called chromatic effect leads to a tune dependence on energy and needs to be corrected with sextupole magnets to make the off-energy electrons remain stable in the storage ring. The chromaticity is defined as the energy-dependent tune variation, and it can be written as,

$$\Delta\nu_{x,y} = \xi_{x,y}\frac{\Delta E}{E}$$
$$\xi_{x,y} = \frac{1}{4\pi}\oint [m_{x,y}(s)\eta_{x,y}(s) + k_{x,y}(s)]\beta_{x,y}(s)ds,$$

where $k_{x,y}$ and $m_{x,y}$ are the quadrupole and sextupole focusing strengths, respectively. The sextupoles are usually installed at large dispersion regions to get an effective chromaticity correction. The magnetic field in sextupole is nonlinear to x or y, and it will generate some aberrations that are ignored in the above expressions of electron motion. These aberrations are very strong and will make the election with small displacement unstable, so more sextupoles (harmonic sextupoles) are intentionally arranged at nondispersion location to cancel the nonlinear driving terms produced by the chromatic sextupoles.

1.3.2 Longitudinal Dynamics

In the light source storage ring, loss in electron energy due to synchrotron radiation is replaced by accelerating cavities, which provide a longitudinal RF voltage in sinusoidal variation by $V(t) = V_c \sin(\omega_{RF}t)$. Here, V_c and ω_{RF} are the total voltage and RF frequency of RF cavities, respectively. For the synchronous electrons, they pass through the accelerating cavities at the synchronous RF phase ϕ_s, and gain an energy of U_0 in one turn,

$$U_0 = \Delta W_0 = eV_c \sin\phi_s,$$

where U_0 is the energy loss per turn of the synchronous electrons at on-energy E_0 due to synchrotron radiation. For the off-energy electrons circulating in the storage ring, they gain the energy,

$$\Delta W = eV_c \sin(\omega_{RF}(t - t_s) + \phi_s)$$

and make one revolution with a path deviation,

$$\frac{\Delta C}{C} = \alpha_c \frac{\Delta E}{E}.$$

In this case, the synchrotron oscillation occurs because they travel in different paths and arrive at the RF cavity at different phases depending on the energy of electrons. The higher energy electron travels on a longer path and arrives at the RF cavity late and therefore gains less energy from the cavity, and vice versa for the low energy electrons. This is the so-called phase-focusing mechanism.

Furthermore, since the higher energy electron radiates more energy due to the radiation property mentioned, one finds that there is a damping effect to this synchrotron oscillation. In this situation, the damped energy oscillation equation can be derived as,

$$\frac{d^2\Delta E}{dt^2} + 2\alpha_\varepsilon \frac{d\Delta E}{dt} + \frac{\alpha_c}{E_0 T_0}[eV_c \sin(\omega_{RF}(t - t_s) + \phi_s) - U_0] = 0.$$

In small amplitude energy oscillation,

$$\frac{d^2\Delta E}{dt^2} + 2\alpha_\varepsilon \frac{d\Delta E}{dt} + \omega_s^2 \Delta E = 0$$

the solution is,

$$\Delta E(t) = \Delta E_0 e^{-\alpha_\varepsilon t} e^{i\omega_s t}$$

with

$$\omega_s = \omega_0 \sqrt{-\frac{\alpha_c h_{rf} e V_c \cos\phi_s}{2\pi E_0}}$$

$$\alpha_\varepsilon = \frac{1}{2T_0}\frac{dU}{dE},$$

where ΔE is the deviation of the electron energy from the energy of synchronous electrons, ω_s is the synchrotron oscillation frequency, α_ε is the energy oscillation damping coefficient, $h_{rf} = \omega_{rf}/\omega_0$ is an integer called the storage ring harmonic number, and $T_0 = 2\pi/\omega_0$ is the revolution time for high relativistic electrons in the storage ring. In large-amplitude energy oscillation, one can find the energy acceptance,

$$\frac{\Delta E_{max}}{E_0} = \sqrt{\frac{U_0}{\pi \alpha_c h_{rf} E_0} F(q)}$$

with

$$F(q) = 2\left[\sqrt{q^2 - 1} - \arccos\left(\frac{1}{q}\right)\right],$$

where $q = eV_c/U_0$ is the overvoltage factor.

1.3.3 Synchrotron Radiation Effects and Beam Dimensions

In a storage ring, the emission of a photon due to synchrotron radiation excites an electron that is performing a new synchrotron and betatron oscillation. This phenomenon is called quantum effects. However, this energy loss and compensation process results in damping the synchrotron and betatron oscillations of the circulating electrons. The balance of these quantum excitation effects and radiation damping effects determines the equilibrium energy spread, emittance, and the beam dimensions, which are of high interest not only to accelerator scientists but also to user scientists.

In longitudinal direction, the damping results from the higher energy electron that radiates more energy in one turn. In the ring, electrons with an energy deviated from the synchronous energy E_0 will emit a total energy U in one turn, and it can be expressed as,

$$U = \frac{1}{c}\oint P_{\mathrm{s}}\left(1 + \frac{\eta(s)}{\rho(s)}\frac{\Delta E}{E}\right)ds.$$

In terms of the change in radiated energy, the energy oscillation damping coefficient can be written as,

$$\alpha_\varepsilon = \frac{1}{\tau_\varepsilon} = J_\varepsilon \frac{U_0}{2T_0E_0}$$

where τ_ε is the damping time and J_ε is the synchrotron partition number,

$$J_\varepsilon = 2 + D$$

with

$$D = \frac{\oint \frac{\eta(s)}{\rho(s)}[\Delta - 2k(s)]ds}{\oint \frac{ds}{\rho^2(s)}},$$

where $k(s)$ is the quadrupole gradient in the magnet, and Δ is determined by the type of dipole magnet,

$$\Delta = \begin{cases} \dfrac{1}{\rho^2(s)} & \text{for sector dipole} \\ 0 & \text{for rectangular dipole} \end{cases}.$$

Normally, when D is a small quantity, the damping rate can be simply approximated as,

$$\alpha_\varepsilon = \frac{U_0}{T_0E_0} = \frac{\langle P_s\rangle}{E_0}.$$

The above formula means that the synchrotron radiation damping time, the inverse damping coefficient, is the time taken by an electron to radiate all its energy away.

The transverse damping occurs due to the synchrotron radiation and the RF acceleration only compensates the longitudinal energy loss of the radiation; the horizontal and vertical damping coefficients are defined respectively as,

$$\alpha_x = \frac{1}{\tau_x} = J_x \frac{U_0}{2T_0E_0}$$

and

$$\alpha_y = \frac{1}{\tau_y} = J_y \frac{U_0}{2T_0E_0},$$

where τ_x and τ_y are the horizontal and vertical damping time, $J_x = 1 - D$ is the horizontal partition number and $J_y = 1$ is the vertical partition number.

Considering the equilibrium between the above radiation damping and quantum excitation, one can find the energy spread as follows,

$$\left(\frac{\sigma_E}{E}\right)^2 = C_q \frac{\gamma^2 \langle 1/\rho^3 \rangle}{J_\varepsilon \langle 1/\rho^2 \rangle}.$$

Since the energy oscillation of the electron is associated with its longitudinal oscillation around the bunch center, the bunch length can be given by,

$$\sigma_l = \frac{c\alpha_c}{\omega_s} \frac{\sigma_E}{E}.$$

In the 3.5 GeV SSRF case with the RF frequency $f_{RF} = 499.65$ MHz and the storage ring harmonic number $h_{rf} = 720$, the damping times are $\tau_x = 7.1$ ms, $\tau_y = 7.0$ ms, and $\tau_\varepsilon = 3.5$ ms. The energy spread is 9.8×10^{-4}, and the momentum compaction factor $\alpha_c = 4.3 \times 10^{-4}$. At the RF voltage of 4.5 MV, the synchrotron oscillation frequency $f_s = \omega_s / 2\pi$ is 5.3 kHz, and the zero current bunch length is 3.7 mm.

In a storage ring, the synchrotron radiation causes a quantum emission of photons, which leads to an increase in betatron oscillation amplitudes of electrons. This antidamping mechanism tends to increase the beam size and divergence, but it is balanced by a damping effect provided by the RF acceleration in the storage ring. These two effects result in an equilibrium emittance, beam size, and divergence in the storage ring. These beam parameters are determined by the lattice and synchrotron radiation effects, and they have no relation with their dynamic history. The resulting natural emittance is,

$$\varepsilon_{x0} = C_q \gamma^2 \frac{\langle H(s)/\rho^3 \rangle}{J_x \langle 1/\rho^2 \rangle}$$

where,

$$C_q = \frac{55}{32\sqrt{3}} \frac{hc/2\pi}{m_0 c^2} = 3.84 \times 10^{-13}\,\mathrm{m}$$

$$H(s) = \gamma_x \eta^2 + 2\alpha_x \eta\eta' + \beta_x \eta'^2,$$

where J_x is the horizontal partition number and $H(s)$ is the dispersion invariant.

To reduce the natural emittance, one needs to increase J_x or decrease the average value of $H(s)/\rho$. J_x can be increased by using gradient dipole magnets, and the average value of $H(s)/\rho$ can be reduced by damping wigglers or using longitudinal gradient dipole magnets.

In a normal storage ring, there is no dispersion in the vertical plane, which results in a near zero vertical emittance. However, the errors of the lattice magnetic fields generate a coupling between horizontal and vertical motions of electrons, which determines a vertical emittance. The coupling factor k is defined as the ratio of vertical emittance ε_y to a horizontal one ε_x, and the relations with natural emittance are

$$\begin{cases} \varepsilon_x = \dfrac{1}{1+k}\varepsilon_{x0} \\ \varepsilon_y = \dfrac{k}{1+k}\varepsilon_{x0} \end{cases}$$

then the beam sizes

$$\begin{cases} \sigma_x = \sqrt{\beta_x \varepsilon_x} = \left[\dfrac{\beta_x C_q}{1+k} \dfrac{\gamma^2}{J_x} \dfrac{\langle H/\rho^3 \rangle}{\langle 1/\rho^2 \rangle} \right]^{\frac{1}{2}} \\ \sigma_y = \sqrt{\beta_y \varepsilon_y} = \left[\dfrac{k\beta_x C_q}{1+k} \dfrac{\gamma^2}{J_x} \dfrac{\langle H/\rho^3 \rangle}{\langle 1/\rho^2 \rangle} \right]^{\frac{1}{2}} \end{cases}.$$

For an electron beam with Gaussian distribution, the standard distribution deviations of amplitudes and angular divergences of electron motion, the beam size, and divergence in horizontal and vertical planes are,

$$\begin{aligned} \sigma_x &= \sqrt{\varepsilon_x \beta_x + \eta^2 \left(\frac{\sigma_E}{E} \right)^2} \\ \sigma_{x'} &= \sqrt{\frac{\varepsilon_x}{\beta_x} + \eta'^2 \left(\frac{\sigma_E}{E} \right)^2} \\ \sigma_y &= \sqrt{\varepsilon_y \beta_y} \\ \sigma_{y'} &= \sqrt{\varepsilon_y / \beta_y}. \end{aligned}$$

In the normal operation of the SSRF storage ring at 3.5 GeV, its natural emittance ε_{x0} is 3.9 nm-rad. It results in ε_x and ε_y being ~3.88 nm-rad and 23 pm-rad at a coupling of 0.6%, with β_x and β_y are 3.6 m and 2.5 m, η and η' are 0.1 m and 0 in the standard straight section, the σ_x and σ_y are 157 and 7.7 μm, σ'_x and σ'_y are 32 and 3 μrad, respectively.

1.3.4 Radiation Source Parameters

Spectral brightness B, a key figure of merit of the light source, is defined as the radiated photon flux density in the six-dimensional phase space volume and can be expressed as,

$$B = \frac{\dot{N}_{\text{ph}}}{4\pi^2 \Sigma_x \Sigma_{x'} \Sigma_y \Sigma_{y'} \Delta\omega/\omega},$$

where Σ_x, $\Sigma_{x'}$, Σ_y, and $\Sigma_{y'}$ are the transverse photon beam size and divergence in horizontal and vertical planes, $\Sigma_x \Sigma_{x'}$ and $\Sigma_y \Sigma_{y'}$ are convolutions between the diffraction-limited photon radiation emittance and the transverse electron beam emittance; the total emittance is given by the product of the rms beam size and divergence, which is

$$\Sigma_{x,y} \Sigma_{x',y'} = \sqrt{\sigma_r^2(\lambda) + \sigma_{x,y}^2} \cdot \sqrt{\sigma_{r'}^2(\lambda) + \sigma_{x',y'}^2}.$$

The radiation properties are determined by the source of radiation, the electron beam parameters, and the radiation wavelength of interest. For the undulator radiation generated by a single electron, the rms photon radiation source, size,

and divergence at wavelength λ are,

$$\sigma_r(\lambda) \approx \frac{\sqrt{2\lambda L_u}}{2\pi}$$
$$\sigma_{r'}(\lambda) \approx \sqrt{\frac{\lambda}{2L_u}},$$

where L_u is the length of the undulator, and its intrinsic radiation emittance can be expressed as,

$$\varepsilon_r(\lambda) = \sigma_r(\lambda)\sigma_{r'}(\lambda) = \frac{\lambda}{2\pi}.$$

By minimizing the total emittance to maximize the spectral brightness of the radiation from the undulator installed at the dispersion-free straight section in the storage ring, one can find the condition,

$$\beta_x = \frac{L_u}{\pi}.$$

It is clear that the brightness will be dominated by the electron beam emittance in the case $\varepsilon_{x,y} \gg \varepsilon_r(\lambda) = \lambda/2\pi$, and the brightness can always be increased by reducing the electron beam emittance till $\varepsilon_r(\lambda)/2$, the so-called diffraction-limited value. In the dispersion-free straight section,

$$\varepsilon_{x,y} = \sigma_{x,y}\sigma_{x'y'} < \frac{1}{2}\varepsilon_r(\lambda) \approx \frac{\lambda}{4\pi}.$$

For the X-ray light source of producing a typical photon energy of 10 keV, the diffraction-limited electron beam emittance that is required to maximize the brightness is around 10 pm, which is two orders of magnitude smaller than that in the horizontal plane of current best third generation light source, but it has been achieved at the vertical plane. Most of the new light source storage ring designs now are pursuing the electron beam emittance ~100 pm-rad or even ~10 pm-rad. They are under development toward achieving the diffraction-limited condition, and they can make the radiation from a flat beam cross-section into a circular shape beam cross-section and even toward the round beam by adjusting the coupling and betatron functions, as shown in (Figure 1.6).

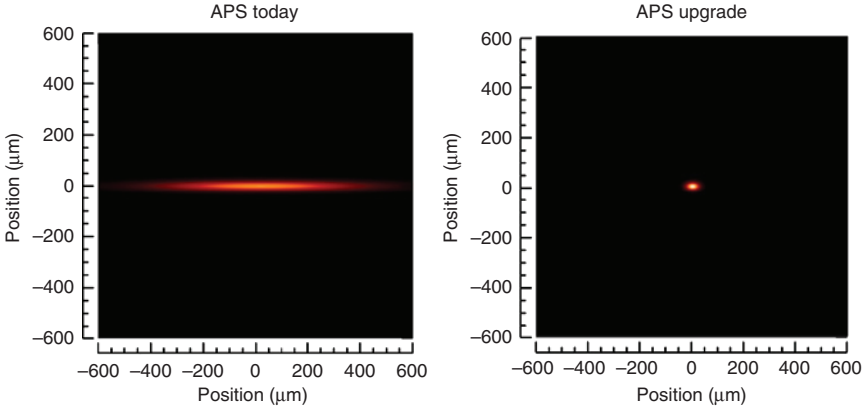

Figure 1.6 The photon beam cross-section of APS today and APS upgrade [16].

In addition, coherent fraction is defined as another figure of merit to measure the transverse radiation quality, and is written as,

$$f_{\text{coh}} = \frac{\varepsilon_r^2(\lambda)}{\Sigma_x \Sigma_{x'} \Sigma_y \Sigma_{y'}}.$$

Reducing electron beam emittance can effectively increase the coherent fraction of radiation, and the full coherence can be approached when diffraction-limited value of emittance is achieved.

1.4 Low-Emittance Lattice for Light Source Storage Ring

Over the past 40 years, the low-emittance lattice has been the core issue in the synchrotron light source development [16–32]. The first low-emittance lattice for light source storage rings was initiated during the design of NSLS at BNL in the late 1970s [25], when the so-called Chasman–Green (CG) structure, containing many double-bending magnets based achromatic arcs connected by zero dispersion straight sections, came into use and commenced a new era in the design and construction of synchrotron light source. Based on the CG structure, the optimization for reducing the emittance has continuously evolved with DBA, TBA, and even QBA structures [25–27] to obtain the emittance from ~100 nm-rad down to ~1 nm-rad to achieve high photon brightness and high flux over the past three or more decades. Now, a new era of synchrotron light source begins with the construction and operation of the ultralow-emittance storage ring based on MBA lattice [18] to approach the diffraction limits at hard X-ray regions.

1.4.1 The Lattice Cell and Its Design Constraints

The storage ring lattice structure of the synchrotron light source is usually built on a so-called lattice cell by repeating itself until a complete circle is formed. Each cell contains an arc section and a straight section. The arc section consists of a number of bending, quadrupole, and sextupole magnets that are arranged in a sequence to regulate and restrict the electron circulating in the storage ring. The straight sections are designed for accommodating injection elements, RF cavities, and insertion devices, which normally range from 2 to 12 m in length.

Besides the photon spectral range user required and the number of insertion device beamlines the light source can accommodate, the lattice design of a light source storage ring is mainly driven by pursuing high photon brightness and high flux from its insertion devices. Meanwhile, it has taken several decades of persistent efforts to minimize the lattice emittance and match its optimized lattice functions with the high-performance undulators and wigglers. Since the emittance is completely determined by the electron energy, bending fields, and lattice functions, low emittance requires a large bending radius and a small value dispersion function and its derivative, which implies that a weak bending field from a large number of short dipole magnets and a strong focus from quadrupoles are required. Strong quadrupole focusing brings stronger chromatic effects, and, in turn, the strong sextupole focusing is required to make the correction of the ring chromaticities for suppressing instabilities and controlling tune shifts of off-energy particles. In the meantime, the so-called

harmonic sextupoles are used to cancel the nonlinear beam dynamics driving terms generated by the chromatic sextupoles for achieving reasonable dynamic apertures.

For a given electron energy, there are a few ways that can be adopted to reduce the emittance [16–32], including (i) increasing the number of bending magnets, (ii) using gradient dipole magnets, (iii) using finite dispersive straight sections, (iv) employing damping wigglers, and (v) increasing the horizontal focusing with high gradient quadrupoles and sextupoles. However, on the other side, there are some constraints to minimize the ring emittance: (i) the dynamic aperture required by beam lifetime and injection efficiency limits the magnetic layout to be perfectly ideal and the quadrupole focusing to be too strong for achieving reasonable chromaticities to control the nonlinear beam dynamics effects, (ii) the lattice functions need to be optimized to meet the insertion device's requirements for maximizing the brightness and flux, such as the beta function at the center of the straight section should be around half of the undulator length, (iii) the practical quadrupole and sextupole strength can be achieved in the currently available technology. Actually, the nonstop minimization of emittance of the light source storage ring has been in progress for the past three decades through both design and engineering efforts.

The main constraints of reaching the theoretical minimum emittance are the dynamic apertures and momentum acceptance limited by the strong focusing effects, namely the nonlinear beam dynamics in the storage ring lattice. Starting from a good linear lattice performance, the nonlinear beam optics is optimized to obtain enough dynamic apertures and momentum acceptance for achieving good beam lifetime and effective beam injection in the storage ring. The lower the emittance the smaller the dynamic apertures, which makes the ultralow-emittance MBA lattice face great challenges in its beam injection and, therefore, a few of new methods, like swap-out, pulse multipoles injection, and longitudinal injection, are proposed and adopted in the new designs. The lattice design and online tuning usually are performed under the help of simulations, using existing methods or codes, such as TRACY, OPA, AT, MADX, ELEGENT, MOGA, MOPSO, FMA, LOCO, and so on.

1.4.2 Typical Lattices for Light Source Storage Ring

The magnetic lattice of a storage ring is the basic building block that determines the characteristics of its circulating electrons. Typical lattice cells used in light source storage rings are illustrated in Figure 1.7.

If a magnetic lattice cell consists of only one nongradient bending magnet with a defecting angle of θ in the storage ring, its theoretical minimum emittance (TME) is,

$$\varepsilon_{x0,\mathrm{TME}} = \frac{1}{12\sqrt{15}} C_q \gamma^2 \theta^3.$$

However, this type of lattice cell does not meet the light source optimization requirements on its beta functions and dispersions at the straight sections, but this can be the building block of the center magnet in the lattice cell. For the typical magnetic lattice structures with two or more bending magnets in each cell

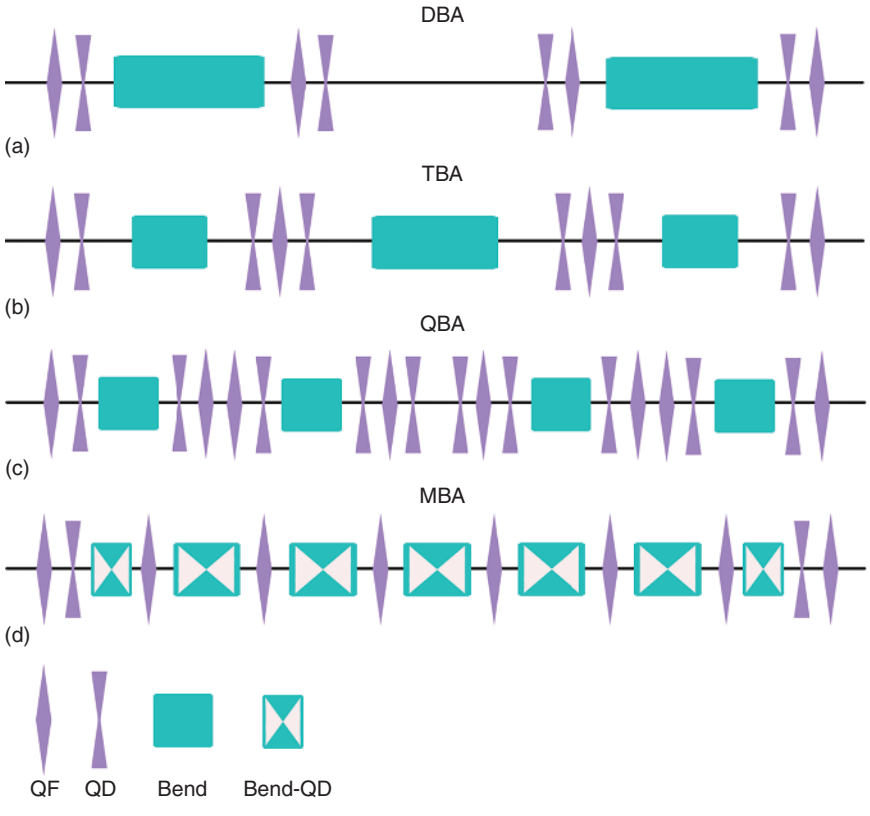

Figure 1.7 Typical types of magnetic lattice cells of light source storage rings (a) DBA, (b) TBA, (c) QBA, (d) MBA.

of real light source storage rings, their lattice cell can be seen as a combination of the DBA lattice cell and the TME lattice cells, and the natural emittance of the magnetic lattice can be expressed as,

$$\varepsilon_{x0} = \frac{Q_F}{J_x}\varepsilon_{x0,\mathrm{TME}} = \frac{Q_F}{J_x}\frac{1}{12\sqrt{15}}C_q\gamma^2\theta^3$$

$$\theta = \frac{2\pi}{MN_c}.$$

where M is the number of bending magnets in a cell, and N_c is the number of lattice cells per storage ring and, therefore, θ is the average deflection angle per bending magnet. J_x can be larger than 1 when using the gradient bending magnet. Q_F is the so-called quality factor of the lattice structure, depending on lattice type, tunes, and dispersion leakage at straights and components space constraints. In a real machine, Q_F is equal to 2–5 with all the practical constraints. By properly shortening the length of the first and last dipole magnets in the lattice cell, which can minimize the emittance, one can find that the theoretical minimum is,

$$\varepsilon_{x0} = \frac{1}{J_x}\frac{1}{12\sqrt{15}}\left(\frac{M+1}{M-1}\right)C_q\gamma^2\theta^3.$$

On employing the same deflection angle to compare these lattices, one can find that the smaller the M the more the number of cells in a storage ring, which means that more straight sections can be obtained for installation of insertion devices. This feature together with the achievable emittance under constraints from nonlinear beam dynamics and component space makes the DBA lattice the dominating one as a third generation light source. This emittance can be further reduced if one relaxes the constraints of zero dispersion at the straights, which many third generation light sources now operate with. The natural emittance of this type of lattice can be reduced by a factor of 3, which leads to an effective emittance, and the contribution of the energy spread through the dispersion at the straight is also effectively reduced by a factor over 2. As an example, Figure 1.8 gives the double-bend lattice cell of the SSRF storage ring.

The SSRF employs a DBA lattice structure with 20 cells, but it operates in a DB configuration with 0.1 m dispersion at the standard straight section; its nominal emittance is 3.9 nm-rad, and a smaller emittance of 2.9 nm-rad at 3.5 GeV (2.1 nm-rad at 3.0 GeV) has been achieved.

As another example, the MAX-IV is the first light source that operates a conventional MBA lattice, which is based on the TME lattice cells in the center matched by two ending dipoles to suppress the dispersion in the straights. The MAX-IV storage ring achieves an emittance of 0.265 nm-rad with 20 7BA cells, about an order lower than that of the DBA with 20 cells. Figure 1.9 is the layout of the MAX-IV 7BA cell.

The conventional MBA lattice has both strong focusing and small dispersion, as a result of which, small dynamic apertures and large chromaticities, constrain it to reach the TME conditions, and therefore the quality factor of emittance needs to stay at a reasonable value. To solve this problem, a so-called hybrid MBA (HMBA), as shown in Figure 1.10, was proposed and applied at the European

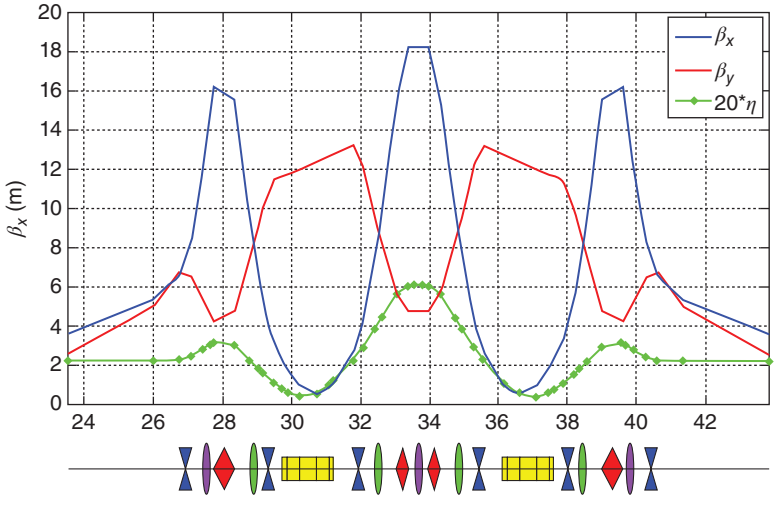

Figure 1.8 The SSRF storage ring lattice cell and dynamic aperture.

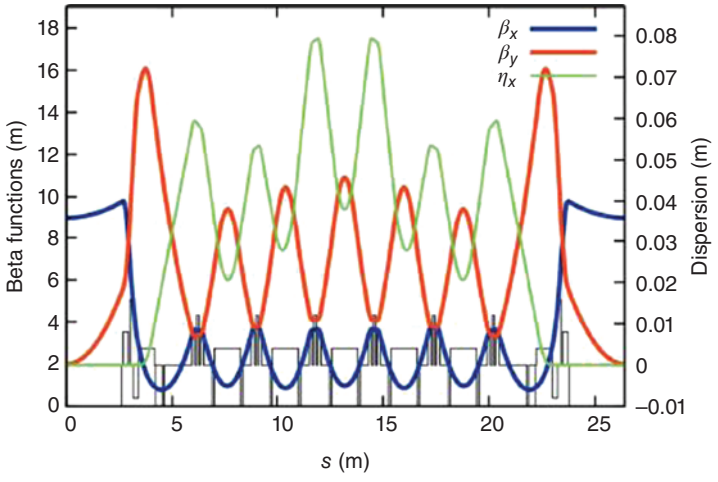

Figure 1.9 The MAX-IV storage ring lattice cell and dynamic aperture [19]. (Erikson 2011 [19]. http://www.trash.net/~leemann/work/ipac11/THPC058.pdf. Licensed under CC BY 3.0.)

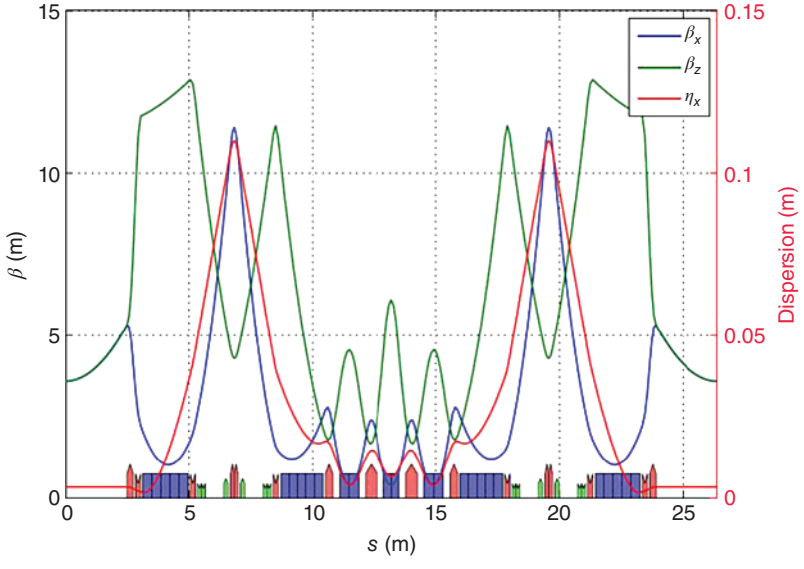

Figure 1.10 The ESRF-EBS HMBA storage ring lattice cell. (Farvacque *et al*. 2013 [20]. http://accelconf.web.cern.ch/AccelConf/IPAC2013/papers/mopea008.pdf. Licensed under CC BY 3.0.)

Synchrotron Radiation Facility (ESRF). This HMBA lattice has two separate β function and dispersion bumps located between the ending dipoles and the first and last inner dipoles of the MBA cell, where sextupoles are placed to ease the chromaticity correction.

Following ESRF-EBS, the new projects, Sirius, APS-U, and high energy photon source (HEPS), chose to use HMBA in their storage ring designs. In addition,

other concepts such as the DDBA/DTBA, longitudinal gradient, and anti-bend lattices were also proposed and have been studied over the past years.

The insertion devices installed at the straight section of storage rings have an impact on the emittance. This effect depends on the local dispersion and magnetic field of IDs and can be characterized by the following formula [33],

$$\varepsilon_{0x,\mathrm{ID}} = (1 + f_{\mathrm{ID}})\varepsilon_{0x}$$

with

$$f_{\mathrm{ID}} = \left(\frac{2\rho^2}{3\pi^2 \rho_{\mathrm{ID}}^3} \frac{\langle H \rangle_{\mathrm{ID}}}{\langle H \rangle} - \frac{\rho}{4\pi \rho_{\mathrm{ID}}^2} \right) \left(\frac{L_{\mathrm{ID}}}{1 + \frac{\rho}{4\pi \rho_{\mathrm{ID}}^2} L_{\mathrm{ID}}} \right),$$

where ρ_{ID} is the radius of the ID magnet, $\langle H \rangle_{\mathrm{ID}}$ is the average of H over the total length of IDs and L_{ID} is the total length of IDs. When $f_{\mathrm{ID}} > 0$, the IDs cause the increase in the storage ring emittance; when $f_{\mathrm{ID}} < 0$, the IDs cause the reduction of the emittance. Therefore, a special ID, the so-called damping wiggler, can be purposely designed and used for reducing the emittance of the light source storage ring.

1.5 Status of Storage Ring Light Sources

Synchrotron light source has experienced three generation's development since the late 1960s [10, 32, 34, 35]. Now, with the MBA lattice based storage rings that was started in 2016, it has entered a new phase, the fourth generation era. However, the third generation light sources are still the work horses and provide the user communities with the electromagnetic radiation ranging from IR to hard X-ray mainly by accommodating various insertion devices in storage rings. There are about 30 third generation light sources in operation worldwide, serving more than 30 000 users each year in total from various research fields.

The early third generation light sources fell into two different energy groups, a high-energy one (6–8 GeV) for generating hard X-ray radiation, and a low-energy one ($\leq$2.0 GeV) for generating vacuum-ultraviolet and soft X-ray radiation. However, along with the advancement of undulators, intermediate energy storage rings ($\sim$2.5–3.5 GeV) [33] based light sources became the preferred choice in this century, as they are cost-effective and can meet most of the users' requirements, with X-ray performance approaching that of the high-energy facilities in the photon energy range of 10–20 keV.

The recent trend toward a new generation synchrotron light source was triggered by the construction of MAX-IV in Sweden, which is the first light source with MBA (7BA) lattice based storage ring. With new concepts and technical advances in on-axis injection, high-focusing gradient magnets, and small aperture vacuum chamber, this kind of storage ring can offer very strong focusing and let the electron beam circulate in its vacuum chamber with very small physical and dynamic apertures, and therefore can achieve over an order of magnitude of lower horizontal emittance, or two or three orders of magnitude of higher brightness, than that available in current operating machines. This MBA based storage

ring approach toward the diffraction limit at the required radiation wavelength is now widely considered and applied to new synchrotron light sources under construction or in the plan phase, from high-energy machines, through intermediate energy to low energy ones.

1.5.1 High Energy Storage Rings

High-energy storage ring light sources are designed and constructed for producing hard X-ray radiation through the fundamental undulator harmonic while keeping the critical wavelength of the bending magnet radiation at ~0.1 nm. Their photon energies cover the range of 1–100 keV [36]. The ESRF at Grenoble was the first X-ray third generation storage ring, commissioned in 1992 and became operational in 1994 [37]. Its user experimental operation was followed by APS in 1996 and SPring-8 in 1997 [34]. With large capacities, these three high-energy light sources accommodate 30–50 undulator beamlines each, providing highly stable and reliable operation for the past 20 years. Besides the emittance reduction by using distributed dispersion and implementation of top-up operation, ESRF and APS have executed major upgrades to achieve high brightness and to install more undulators. And now, ESRF and APS are making new upgrade projects, called ESRF-EBS and APS-U, to enhance the brightness by a factor up to 100. They are constructing 7BA lattice based storage rings to replace the old ones in the existing accelerator tunnel, aiming at being operational for user experiments by 2020–2023 [38, 39]. SPring-8 is planning similar upgrades to generate brighter X-rays [40].

Although expensive, the high-energy ring offers higher brightness in the hard X-ray region. A recent example the PETRA-III, converted from the high-energy physics machine PETRA built in the late 1970s at DESY, is a 6 GeV hard X-ray synchrotron source commissioned in 2009, and opened for user experiments in 2010 [41]. In PETRA-III, one octant of the storage ring is reconstructed with a DBA magnetic lattice structure providing nine straight sections, which accommodates 27 beamlines. The achieved horizontal emittance with damping wigglers is 1 nm-rad, and the top-up mode is used for routine operation.

Furthermore, there is still a strong interest in building new high-energy light sources. For example, a 6 GeV high energy photon source, namely HEPS, with 7BA lattice based storage ring with a circumference of 1.3 km [42] is under development in Beijing, China, aimed at opening to user experiments in 2025. Beyond the above activities, an idea to convert PEP-II collider to 6 GeV and 10 pm-rad emittance light source, called PEP-X, was proposed at SLAC [43], and another plan to upgrade PETRA-III into a diffraction limited storage ring light source PETRA-IV at 0.1 nm is now under study at DESY, targeted to achieve 200 mA beam current and 10 pm-rad emittance at 6 GeV for user experiments in 2026 [44]. Table 1.1 is a parameter summary of these high-energy light sources.

1.5.2 Low Energy Storage Rings

Low-energy third generation storage rings for producing VUV and soft X-ray radiation to investigate the electronic and chemical structures of matter were developed simultaneously with high-energy ring sources and came on line

Table 1.1 A parameter summary of high-energy storage ring light sources.

Light source	Energy (GeV)	Circumference (m)	Emittance (nm rad)	Current (mA)	Straight sections	Operation year/status
ESRF	6.0	844.4	4	200	32 × 6.3 m	1994
APS	7.0	1104	3	100	40 × 5.8 m	1996
SPring-8	8.0	1436	2.8	100	44 × 6.6 m, 4 × 30 m	1997
PETRA-III	6.0	2304	1.0 (DW)	100	1 × 20 m, 8 × 5 m	2010
ESRF-EBS	6.0	844.4	0.15	200	32 × 5.0 m	Construction
APS-U	6.0	1104	0.065	200	40 × 5.8 m	Construction
HEPS	6.0	1295	~0.059	200	48 × 6.0 m	Planning/R&D
SPring-8 II	6.0	1435.5	0.14	200	44 × 4.7 m, 4 × 30 m	Planning
PETRA-IV	6.0	2304	0.01–0.03	100		Planning
PEP-X	6.0	2200	0.01	200		Concept

around 1990. Super-ACO at Orsay, based on an 800 MeV storage ring optimized with low emittance and installation of insertion devices, was commissioned in 1987 [45], and it was regarded as the first third generation light source. And in 1993, the ALS based on a 1.9 GeV storage ring became operational [46], and was followed by ELETTRA, TLS, PLS, LNLS, MAX-II, and BESSY-II in the 1990s [35]. In the 2000s, New SUBARU, SAGA-LS DELSY, and MAX-III came online [47]. Table 1.2 shows a parameter summary of the low-energy light source storage rings.

Development of low-energy storage rings has been progressing in two directions. One is upgrading the existing facilities to higher performance. For example, the ALS upgrade [48] includes modifying the lattice by increasing the horizontal tune from 14.25 to 16.25, increasing dispersion in the straight to 0.15 m to reduce the emittance to 2.1 nm-rad, and replacing RF cavities with HOM-damped ones. The ELETTRA upgrade includes a new dedicated full energy booster injector for top-up operation. The HLS-II upgrade was completed by reconstructing a brand new storage ring and a full energy linac injector in the existing bunkers. Further on, the BESSY-II is making an upgrade of variable pulse length storage ring called BESSY VSR, aiming at being operational for user experiments in 2020 [49]. The other direction is constructing new light sources. For example, the Demark's ASTRID 2 and the central Japan synchrotron radiation facility [50, 51] started user service in 2012. The Polish Synchrotron Light Source (SOLARIS/1.5 GeV) was constructed and was commissioned in 2015 [52], and the MAX-IV/1.5 GeV storage ring was commissioned in 2016 [53].

The low-energy MBA based storage ring light source is also under active development. The ALS-U based on 9BA storage ring lattice is in the CD0 phase, by replacing the existing ALS with a new machine of 50 pm-rad emittance at 2.0 GeV in the same tunnel [54]. The ELETTRA 2.0 was considered as an upgrade based on 6BA lattice storage ring at 2 GeV to reduce its current horizontal emittance by a factor of 10 [55]. And a new low-energy facility called Hefei advanced light source (HALS) [56], with a 2.0 GeV storage ring based on 6BA lattice, is proposed in China, Table 1.2 is a parameter summary of the low-energy light source storage rings.

1.5.3 Intermediate Energy Storage Rings

Intermediate energy third generation storage rings came online as cost-effective light sources from the beginning of this century, taking advantage of the technological advancement in insertion devices and accelerator technologies. These storage rings utilize low emittance beams at an energy of ~2.5–3.5 GeV to produce photon beams in the hard X-ray region with an emphasis on 10–20 keV, through high (up to 13th) harmonic radiations of short period (~20 mm) and mini gap (minimum at 4–5 mm) in-vacuum undulators. This combination helps greatly to reduce the light source cost and offers the possibility and flexibility to distribute high-performance hard X-ray sources in many locations all over the world.

SLS was the first intermediate energy light source conceived under these ideas from its initial design stage and operated for user experiments in 2000 [57].

Table 1.2 A parameter summary of low-energy light source storage rings.

Light source	Energy (GeV)	Circumference (m)	Emittance (nm rad)	Current (mA)	Straight sections	Operation year/status
ALS	1.9	196.8	2.1	400	12 × 6.7 m	1993
ELETTRA	2.0/2.4	259	7	300	12 × 6.1 m	1994
TLS	1.5	120	25	240	6 × 6 m	1994
LNLS	1.37	93.2	70	250	6 × 3 m	1997
BESSY-II	1.7	240	6.1	200	8 × 5.7 m, 8 × 4.9 m	1999
New SUBARU	1.5	118.7	38	500	4 × 2.6 m, 2 × 14 m	2000
SAGA-LS	1.4	75.6	7.5	300	8 × 2.93 m	2005
CJSRF	1.2	72	53	300		2013
ASTRID2	0.58	45.7	10.0	200	6 × 2.9 m	2013
HLS-II	0.8	66.0	38	300	4 × 4.2 m, 4 × 2.3 m	2015
Solaris	1.5	96	6.0	500	12 × 3.5 m	Commissioning
MAX-IV/1.5	1.5	96	6.0	500	12 × 3.5 m	Commissioning
ALS-U	2.0	196.5	0.109	500	12 × 6.7 m	Planning
ELETTRA 2.0	2.0	259	0.28	400	12 × 6.1 m	Concept
HALS	2.0	396	0.047	500	24 × 5.2 m	Concept

Table 1.3 A parameter summary of the intermediate energy light source storage rings.

Light source	Energy (GeV)	Circumference (m)	Emittance (nm.rad)	Current (mA)	Straight sections	Operation year/status
SLS	2.4–2.7	288	5	400	3 × 11.7 m, 3 × 7 m, 6 × 4 m	2001
ANKA	2.5	110.4	50	200	4 × 5.6 m, 4 × 2.2 m	2002
CLS	2.9	170.88	18.1	500	12 × 5.2 m	2003
SPEAR-3	3.0	234	12	500	2 × 7.6 m, 4 × 4.8 m, 12 × 3.1 m	2003
SOLEIL	2.75	354.1	3.74	500	4 × 12 m, 12 × 7 m, 8 × 3.8 m	2007
DIAMOND	3.0	561.6	2.7	300	6 × 8 m, 18 × 5 m	2007
ASP	3.0	216	7–16	200	14 × 5.4 m	2007
INDUS-II	2.5	172.5	58	300	8 × 4.5 m	2008
SSRF	3.5	432	3.9	300	4 × 12 m, 16 × 6.5 m	2009
ALBA	3.0	268.8	4.5	400	4 × 8 m, 12 × 4.2 m, 8 × 2.6 m	2011
PLS-II	3.0	281.82	5.9	400	10 × 6.86 m, 11 × 3.1 m	2012
NSLS-II	3.0	780	0.6 (DW)	400	15 × 8 m, 15 × 5 m	2014
TPS	3.0	518.4	1.7	400	6 × 11.7 m, 18 × 7 m	2014
MAX-IV	3.0	528	0.3 (DW)	500	20 × 5 m	2015
SESAME	2.5	133.12	26	400	8 × 4.44 m, 8 × 2.38 m	2017
SIRIUS	3.0	518.4	0.15	350	10 × 7 m, 10 × 6 m	Construction
ILSF	3.0	528	0.48	400	20 × 5.1 m	Planning
SLS-II	2.4	288	0.13	400	3 × 10 m, 3 × 5.7 m, 6 × 3.2 m	Planning
CANDLE	3.0	268.8	0.43	500	16 × 4.4 m	Concept
Diamond II	3.0	561.6	0.12	300	6 × 8 m, 18 × 5 m, 24 × 3 m	Concept
SLiT-J	3.0	353	0.92	500	16 × 5.44 m, 16 × 1.84 m	Concept
KEK-LS	3.0	570	0.13	500	20 × 5.6 m, 20 × 1.2 m	Concept
TURKAY	3.0	477	0.51	500	20 × 5.0 m	Concept
SOLEIL II	2.75	354	0.14	500	16 × 9.5 m	Concept
SSRF-U	3.0	432	0.2	300	16 × 5.6 m, 4 × 10.4 m	Concept

It is followed that many intermediate energy storage ring light sources [35, 58] were designed and constructed. ANKA, CLS, SPEAR3, ASP, SOLEIL, DIAMOND, INDUS-II, and SSRF became operational before 2010. ALBA, PLS-II (PLS upgrade at 3 GeV), NSLS-II and TPS [35] were constructed and became operational before 2017. The performance of the intermediate energy light source has been improved dramatically over the past 20 years and has entered a new level. The horizontal emittance is reduced from ~10 nm-rad to less than 5 nm-rad and then to sub nanometer radian level. The NSLS-II storage ring has realized the horizontal emittance of 0.9 nm-rad and the vertical emittance of 6 pm-rad by using damping wigglers [59], and its associated brightness has reached over 10^{21} photons s^{-1} mm^{-2} $mrad^{-2}$ (0.1% BW)$^{-1}$. Further on, the 3 GeV MAX-IV storage ring, which successfully pioneers the MBA (7BA) lattice, has been commissioned and has realized the horizontal emittance of 340 pm-rad and the vertical emittance of 15.7 pm-rad without damping wigglers [60], which predicates a brightness over 10^{22} photons s^{-1} mm^{-2} $mrad^{-2}$ (0.1% BW)$^{-1}$. The 5BA based Sirius light source facility, designed with a similar performance as MAX-IV, is now under construction at LNLS, aimed at being operational for user experiment in 2019 [61].

The momentum of the intermediate energy light source development still keeps strong, as evidenced not only by the project approaching commissioning like SESAME, but also by many new project plans and proposals based on MBA lattice, including the new green-field projects, such as the Iran Light Source Facility [62], TURKAY [63], SLiT-J [64], and KEK-LS [65], and upgrade projects such as Diamond-II and SLS2.0 [21, 24]. In addition, there are also many future upgrade considerations under study, such as SOLEIL and SSRF-U, to convert the existing facilities into the fourth generation synchrotron light sources [66–68]. Table 1.3 shows a parameter summary of the intermediate energy light source storage rings.

References

1 Winick, H. (1994) *Synchrotron Radiation Sources, A Primer*, World Scientific.
2 Hofmann, A. (2004) *The Physics of Synchrotron Radiation*, Cambridge University Press.
3 Attwood, D. (2007) *Soft X-rays and Extreme Ultraviolet Radiation: Principle and Applications*, Cambridge University Press.
4 (a) Wiederman, H. (2003) *Synchrotron Radiation*, Springer-Verlag; (b) Wiederman, H. (2007) *Particle Accelerator Physics*, 3rd edn, Springer-Verlag.
5 Duke, P.J. (2000) *Synchrotron Radiation*, Oxford University Press.
6 Clarke, J.A. (2004) *The Science and Technology of Undulators*, Oxford University Press.
7 Onuki, H. and Elleaume, P. (2003) *Undulators, Wigglers and Their Application*, Taylor and Francis.
8 Sands, M. (1977) The physics of storage rings: an introduction. SLAC-121.
9 Wille, K. (2000) *The Physics of Particle Accelerators, An Introduction*, Oxford University Press.

10 Zhao, Z.T. (2010) Storage ring light sources, in *Review of Accelerator Science and Technology*, vol. **3**, World Scientific Publishing Co Pte Ltd., pp. 57–76.
11 Kim, K.-J. (1989) Characteristics of synchrotron radiation. *AIP Proc.*, **184**, 567–631.
12 Murphy, J. (1989) Synchrotron Light Source Data Book. *BNL-42333*, Brookhaven National Lab.
13 Chao, A., Moser, H.O., and Zhao, Z.T. (2002) *Accelerator Physics, Technology and Applications*, World Scientific.
14 Wolski, A. (2013) Low Emittance Machines, CERN Accelerator School, Trondheim, Norway, 2013. *CERN-2014-006*, CERN.
15 Walker, R. (1998) Insertion Devices: Undulators and Wigglers. *CERN 98-04*, CERN, pp. 129–190.
16 Handderson, S. (2017) Advanced Photon Source Upgrade Project: The World's Leading Hard X-ray Light Source, http://www.fnal.gov/pub/colloquium/ (accessed 18 January 2017).
17 Hettel, R. (2014) DLSR design and plans: an international overview. *J. Synchrotron Radiat.*, **21**, 843–855.
18 Borland, M., Decker, G., Emery, L., Sajaev, V., Sun, Y., and Xiao, A. (2014) Lattice design challenges for fourth-generation storage-ring light sources. *J. Synchrotron Radiat.*, **21**, 912–936.
19 Erikson, M. (2011) The MAX-IV synchrotron light source. Proceedings of IPAC11, San Sebastian, Spain, p. 302.
20 Farvacque, L., Carmignani, N. *et al*. (2013) A low-emittance lattice for the ESRF. Proceedings of IPAC13, Shanghai, China, p. 79.
21 Bartolini, R. (2016) Design and optimization strategies of nonlinear dynamics for diffraction limited synchrotron light sources. Proceedings of IPAC16, Busan Korea, p. 33.
22 Hettel, R. (2014) Challenges in the design of diffraction-limited storage rings. Proceedings of IPAC14, Dresden, Germany, p. 7.
23 Borland, M. (2012) Progress towards ultimate storage ring light sources. Proceedings of IPAC12, New Orleans, LA, USA, p. 1035.
24 Streun, A., Aiba, A. *et al*. (2016) Proposed upgrade of the SLS storage ring. Proceedings of IPAC2016, Busan, Korea, p. 2922.
25 Chasman, R., Green, G.K., and Rowe, E.M. (1975) Preliminary design of a dedicated synchrotron radiation facility. *IEEE Trans. Nucl. Sci.*, **22**, 1765–1767.
26 Einfeld, D. and Muelhaupt, G. (1980) Choice of the principal parameters and lattice of BESSY. *Nucl. Instrum. Methods*, **172**, 55–59.
27 Tsumaki, K., Nagaoka, R. *et al*. (1989) Lattice comparison for the 8 GeV synchrotron radiation source. Proceedings of PAC89, Chicago, IL, USA, p. 1358.
28 Einfeld, D., Schaper, J. *et al*. (1995) Design of a diffraction limited light source. Proceedings of PAC95, Dallas, TX, USA, p. 177.
29 Tanaka, H. and Ando, A. (1996) Minimum effective emittance in synchrotron radiation sources composed of modified Chasman–Green lattice. *Nucl. Instrum. Methods Phys. Res., Sect. A*, **369**, 312–321.

30 Lee, S.Y. (1996) Emittance optimization in three- and multipole-bend achromats. *Phys. Rev. E*, **54** (2), 51–54.

31 Teng, L. (1985) Minimum Emittance Lattice for Synchrotron Storage Rings. *ANL/FNAL LS-17*.

32 Corbett, J. and Rabedeau, T. (1999) Intermediate energy storage rings. *Synchrotron Radiat. News*, **12** (6), 25–33.

33 Zhang, Q.L. (2015) Study on the effects of insertion devices at SSRF. PhD dissertation. The University of Chinese Academy of Sciences.

34 Bilderback, D.H., Elleaume, P., and Weckert, E. (2005) Review of third and next generation synchrotron light sources. *J. Phys. B: At. Mol. Opt. Phys.*, **38**, S773–S797.

35 Namkung, W. (2010) Review of third generation light sources. Proceedings of IPAC10, Kyoto, Japan, p. 2411.

36 Buras, B. and Materlik, G. (1986) The European synchrotron radiation facility: an overview. *Nucl. Instrum. Methods Phys. Res., Sect. A*, **246**, 21–31.

37 Filhol, J.-M. (1994) Status of the ESRF. Proceedings of EPAC94, London, England, p. 8.

38 Raimondi, P. (2016) The ESRF low emittance upgrade. Proceedings of IPAC16, Busan, Korea, p. 2023.

39 Handerson, S. (2015) Status of the APS upgrade project. Proceedings of IPAC15, Richmond, VA, USA, p. 1791.

40 Tanaka, H. and Ishikawa, T. (2016) The SPring-8 upgrade project. Proceedings of IPAC16, Busan, Korea, p. 2867.

41 Balewiski, K., Bieler, M. *et al*. (2011) PETRA-III upgrade project. Proceedings of IPAC11, San Sebastian, Span, p. 2948.

42 Xu, G., Duan, Z. *et al*. (2016) Recent physical studies for the HEPS project. Proceedings of IPAC16, Busan, Korea, p. 2886.

43 Cai, Y., Bane, K., Hettel, R. *et al* (2012) Ultimate storage ring based on fourth-order geometric achromats. *Phys. Rev. Spec. Top. Accel Beams*, **15**. doi: 10.1103/physrevstab.15.054002

44 Keil, J. (2016) PETRA-IV lattice studies. 2nd Workshop on Low Emittance Ring Lattice Design, Lund, Sweden, December 1, 2016.

45 Level, M.P. (1987) Progress report on super-ACOI. Proceedings of PAC87, Washington, DC, USA, p. 470.

46 Jackson, A. (1995) Operational experience at the advanced light source. Proceedings of the 1995 SRI Conference, *Rev. Sci. Instrum.*, **66** (9).

47 Kihara, M. (1998) Development of synchrotron radiation storage rings. *J. Sychrotron Radiat.*, **5**, 179–183.

48 Steier, C. (2010) Status of the low emittance upgrade of the advanced light source. Proceedings of IPAC10, Kyoto, Japan, p. 2645.

49 Jankowiak, A., Anders, W. *et al*. (2016) The BESSY VSR project for short X-ray pulse production. Proceedings of IPAC16, Busan, Korea, p. 2883.

50 Moller, S.P. *et al*. (2010) ASTRID2-the new low-emittance light source in Denmark. Proceedings of IPAC10, Kyoto, Japan, p. 2487.

51 Yamamoto, N. *et al*. (2010) Accelerators of the central Japan synchrotron radiation research facility project. Proceedings of IPAC10, Kyoto, Japan, p. 2567.

52 Wawrzyniak, A.I. *et al*. (2016) Solaris storage ring commissioning. Proceedings of IPAC16, Busan, Korea, p. 2895.
53 Sjostrom, M. (2016) MAX-IV ring status. ESLS2016, November 28–30, 2016.
54 Steier, C., Byrd, J. *et al*. (2016) Physics design progress towards a diffraction limited upgrade of the ALS. Proceedings of IPAC16, Busan, Korea, p. 2956.
55 Karantzoulis, E. (2015) ELETTRA 2.0 – the next machine. Proceedings of IPAC15, Richmond, VA, USA, p. 1532.
56 Bai, Z.H., Liu, G.W. *et al*. (2016) Initial lattice design for Hefei advance light source: a VUV and soft X-ray diffraction-limited storage ring. Proceedings of IPAC16, Busan, Korea, p. 2889.
57 Boege, M. (2002) First operation of the Swiss light source. Proceedings of EPAC02, Paris, France, p. 39.
58 Zhao, Z.T. (2007) Commissioning of new synchrotron radiation facilities. Proceedings of PAC07, Albuquerque, NM, USA, p. 17.
59 Willeke, F. (2015) Commissioning of NSLS-II. Proceedings of IPAC'15, p. 11.
60 Eriksson, M., Al-Dmour, D. *et al*. (2016) Commissioning of the MAX-IV light source. Proceedings of IPAC16, Busan, Korea, p. 11.
61 Rodrigues, A.R.D. *et al*. (2016) Sirius status report. Proceedings of IPAC16, Busan, Korea, p. 2811.
62 Rahighi, J., Eghbali, R. *et al*. (2016) Recent progress on the development of ILSF project. Proceedings of IPAC16, Busan, Korea, p. 2861.
63 Aksoy, A., Karsli, O. *et al*. (2016) Accelerator based light source projects of Turkey. Proceedings of IPAC16, Busan, Korea, p. 2936.
64 Hama, H. (2016) Status of SLIT-J. LER2016, Paris, France, October 26–28, 2016.
65 Honda, T., Adachi, M. *et al*. (2016) Present status of KEK photon factory and future projects. Proceedings of IPAC16, Busan, Korea, p. 2871.
66 Nagaoka, R., Brunelle, P. *et al*. (2016) Design consideration of a 7BA–6BA lattice for the future upgrade of SOLEIL. Proceedings of IPAC16, Busan, Korea, p. 2815.
67 Zhao, Z.T., Yin, L.X. *et al*. (2015) Consideration on the future major upgrades of the SSRF storage ring. Proceedings of IPAC15, Richmond, VA, USA, p. 1672.
68 Tian, S.Q., Zhang, M.Z. *et al*. (2015) Lattice design of the SSRF-U storage ring. Proceedings of IPAC15, Richmond, VA, USA, p. 304.